# A 65-nm CMOS Fully Integrated Analysis Platform Using an On-Chip Vector Network Analyzer and a Transmission-Line-Based Detection Window for Analyzing Circulating Tumor Cell and Exosome

Kiichi Niitsu ⬡, *Member, IEEE*, Taiki Nakanishi, *Student Member, IEEE*, Shunya Murakami,
Maya Matsunaga, *Student Member, IEEE*, Atsuki Kobayashi ⬡, *Student Member, IEEE*, Nissar Mohammad Karim,
Jun Ito, Naoya Ozawa ⬡, Tetsunari Hase ⬡, Hiromasa Tanaka ⬡, Mitsuo Sato, Hiroki Kondo, Kenji Ishikawa,
Hidefumi Odaka, Yoshinori Hasegawa, Masaru Hori, *Member, IEEE*, and Kazuo Nakazato, *Member, IEEE*

*Abstract*—A fully integrated CMOS circuit based on a vector network analyzer and a transmission-line-based detection window for circulating tumor cell (CTC) and exosome analysis is presented for the first time. We have introduced a fully integrated architecture, which eliminates the undesired parasitic components and enables high-sensitivity, to analyze extremely low-concentration CTC in blood. The detection window was designed on the high-sensitive coplanar waveguide line. To validate the operation of the proposed system, a test chip was fabricated using 65-nm CMOS technology. Measurements were performed after adding a tiny lump of silicone or a droplet of water on its detection window. The measured results show |S_21| degradation of $-1.96$ dB and $-6.04$ dB for the silicone and the droplet, respectively, at 1.4 GHz. In addition, in another measurement using magnetic beads, it is confirmed that the proposed circuit can analyze even low concentrations of 20 beads/$\mu$L.

As well as microbeads, measurement with CTCs was successfully demonstrated.

*Index Terms*—Circulating tumor cell (CTC), CMOS, coplanar waveguide (CPW) line, dielectric properties, exosome, on-chip VNA.

## I. INTRODUCTION

CANCER is one of the leading causes of mortality worldwide, occupying for 8.8 million deaths in 2015, especially 1.69 million deaths owing to lung cancer according to World Health Organization (WHO). Moreover, it is estimated to increase the number of new cases by approximately 70% for the next two decades.

In order to reduce the risk of cancer, it is generally known that the early detection of cancer cells is very important because treatments become more effective for cancer diagnosed at an early stage. Moreover, the early detection is also likely to render survival rates higher. However, the current method for cancer diagnosis, so-called tissue biopsy, is not very beneficial for early detection. The tissue biopsy is a medical test to examine a sample directly obtained from tumor likely to be cancerous and detect cancer cells by using a microscope. However, the biopsy might be invasive, dangerous and painful; which can be harmful to patient's body and organs. Furthermore, the patient might need to face the pain to go through repeated biopsy processes after the treatment or even if the cancer recurs.

On the other hand, there is one promising approach to improve the early detection of cancer, which is liquid biopsy [1]. The liquid biopsy is a medical procedure conducted on a sample taken from a person's body fluid such as blood and urine to look for cancer cells or a tumor. Hence, the liquid biopsy normally has the potential to achieve non-invasive and rapid diagnosis in addition to the early detection of cancer. What is more, it helps to see if cancer cells are growing or not, being able to monitor the effect of a treatment in real time, as doctors are capable of taking a sample more easily than by tissue biopsy.

TABLE I
EXAMPLES IN SIZE OF CTCs

| Types | Average size |
|---|---|
| H1795 (Lung Cancer) | 11.7 µm |
| NCI-H82 (Lung Cancer) | 12.5 µm |
| SK-BR-3 (Breast Cancer) | Approximately 20 µm |

Examples of biomarkers for the liquid biopsy is circulating tumor cells (CTCs) and exosomes, which are tumor cells detached from primary tumors and circulating in the bloodstream. As mentioned above, CTCs analysis has the possibility to play a crucial role in early cancer detection, monitoring a treatment effect in real time and prognosis of cancerous cells. Table I shows the examples in size of CTCs. The size of CTCs are in the range of 10~20 µm in general, which has usually no relationship between cancer stages.

One of the most critical challenges in CTCs/exosomes analysis is that the CTCs/exosomes concentration is considerably low in blood; therefore, the CTCs/exosomes analysis requires a highly sensitive biosensor to detect the cells signal even in the presence of various noise. There are some approaches to detect CTCs/exosomes which have been studied over the past years [1]–[7].

Over a few decades, biomolecule sensing technique using a microwave has been proposed for its highly sensitive, rapid and reliable measurement [8]–[12]. This is mainly due to the $\gamma$ dispersion which a microwave causes shows a significant variation in the dielectric constant. Another reason for employing a microwave-sensing approach is that a microwave is sorted as non-invasive radiation, leading to non-invasive detection of a living biomolecule.

A label- and antibody-free biosensor using microwave for identifying cancer cells has recently been proposed in a previous study [12]. The biosensor can realize rapid, high-sensitive and accurate tumor cells analysis even at low cell concentrations of 20 cells/µL because it can eliminate the parasitic microwave effects generated from the polarization of cultured medium and substrate material. Compared to conventional impedance measurements, this does not require reference electrode, which is one of the most difficult challenges for guaranteeing accuracy. Nonetheless, the biosensor might not be very clinically practical since its signal process requires an area-consuming and expensive external vector network analyzer (VNA).

This paper proposes a fully-integrated circuit based on CMOS composed with a biosensor referred to the previous study [12] and an on-chip VNA for CTC analysis. The proposal is expected to achieve more accurate and sensitive analysis of CTC owing to the elimination of the undesired parasitic effects from substrate and cables in comparison with other papers [8]–[12].

In addition to the conference proceedings [13], this paper presents detail of the implementation, measurement with CTC,
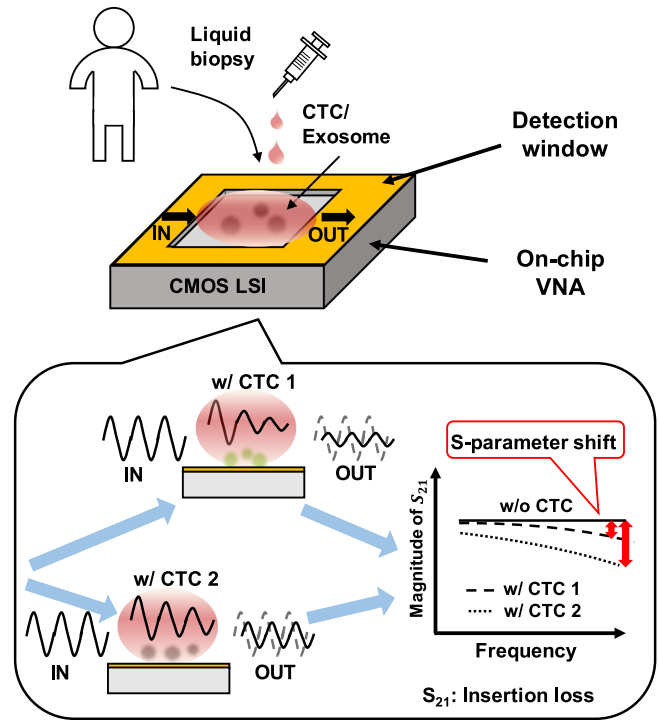


Fig. 1. Conceptual diagram of the proposed CMOS CTC/exosome analysis platform.

and discussions for exosome analysis. Compared to the previous study [14], this paper includes measurement using higher frequency with real CTCs samples, which improves feasibility for practical applications. Section II provides the proposed fully-integrated CTCs/exoxomes analysis system. Section III shows test chip design and measurement setup. Section IV presents discussions for exosome analysis. Section V concludes the paper.

## II. FULLY-INTEGRATED CTCs/EXOSOMES ANALYSIS SYSTEM

Fig. 1 shows a concept image of the proposed architecture for analyzing CTC/exosomes using a CMOS circuit based on microwave. In the figure, $S_{21}$ indicates the insertion loss. When a sinusoidal wave input to the system on which blood samples including CTCs/exosomes are added, there should be variations in a phase and amplitude of the output signal, that is S-parameter, because of the CTCs/exosomes' impedance change by different types and the number of CTCs/exosomes on the detection region. Moreover, the S-parameter can be measured by a part of CMOS integrated circuit. Therefore, there is two main building blocks composing with the proposed architecture: one is a detection area referred to the previous study mentioned above and the other is an on-chip VNA based on CMOS technology for S-parameter measurement. In the following sub-sections, electromagnetic (EM) and SPICE simulations are performed using CST MW Studio and SPICE simulation with 65-nm PDK, respectively.

For practical application, microfluids will be employed for avoiding overflow of the sample liquids and conductivity

Fig. 2. (a) Structure of the detection area, (b) cross section of the detection area, and (c) equivalent circuit of the detection area with CTC (L = 500 $\mu$m, S = 182 $\mu$m, G = 12 $\mu$m, $t_{Cu}$ = 3.4 $\mu$m, and h = 300 $\mu$m).

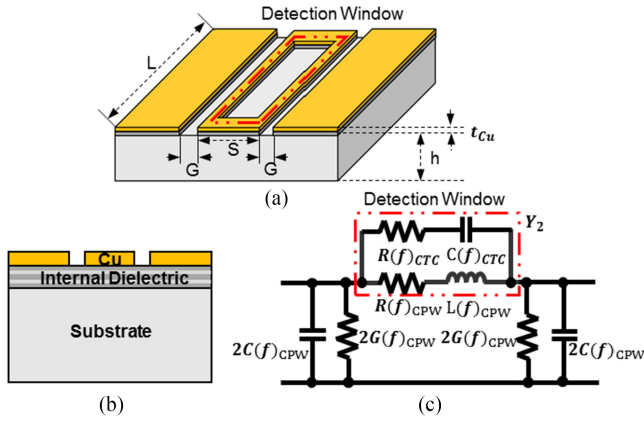changes. Besides, issues of electrostatic discharge (ESD) with HBM/CDM modeling must be addressed.

### A. Detection Area With Transmission-Line-Based Detection Window

Fig. 2(a) describes the structure of the transmission-line-based detection area investigated in [12]. The structure is based on the coplanar-waveguide (CPW) line, which consists of a signal line in the middle and two ground lines at both sides. The biosensor also has a detection window for CTCs/exosomes in the middle of the signal line so that the EM waves concentrated on the signal line significantly penetrate CTCs/exosomes. In Fig. 2(b), the cross section of the detection area is illustrated, which is fabricated on a semiconductor substrate and intermetal dielectric (IMD) and copper composing with the CPW line on the top. Fig. 2(c) shows an equivalent circuit of the detection area including CTCs/exosomes dropped on it. The values of $R(f)_{CTCs}$ and $C(f)_{CTCs}$ correspond to the resistance and capacitance of the CTCs/exosomes, respectively while $R(f)_{CPW}$, $L(f)_{CPW}$, $G(f)_{CPw}$, and $C(f)_{CPW}$ are the lumped-element resistance, inductance, conductance, and capacitance for the CPW line, respectively. In this circuit model, the cell-based parameters of $R(f)_{CTCs}$ and $C(f)_{CTCs}$ represent all of CTCs/exosomes on the detection area. The two cell-based value can be obtained from the transformation between a ABCD matrix and S-parameter matrix:

$$\begin{pmatrix} S_{11} & S_{12} \\ S_{21} & S_{22} \end{pmatrix} \Leftrightarrow \begin{pmatrix} A & B \\ C & D \end{pmatrix}. \tag{1}$$

According to the transformation and the ABCD matrix of the equivalent circuit shown in Fig. 2(c), the following expressions can be derived as follows:

$$B = Z_0\left(f\right) \frac{\left(1 + S_{11}\right)\left(1 + S_{22}\right) - S_{12}S_{21}}{2S_{21}} = \frac{1}{Y_2}, \tag{2}$$

$$Y_2 = \frac{1}{R(f)_{CPW} + j\omega L(f)_{CPW}} + \frac{1}{R(f)_{CTC} + \frac{1}{j\omega C(f)_{CTC}}}, \tag{3}$$
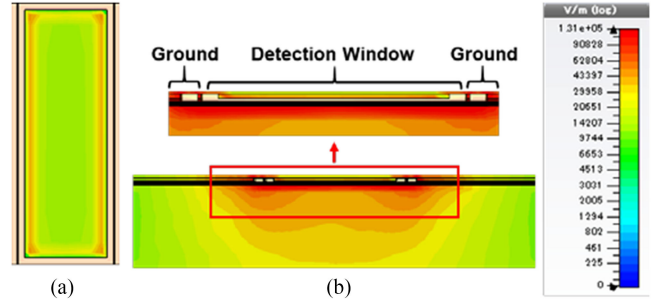


Fig. 3. Electrical field distribution (a) top-down view of the unloaded detection area, (b) cross section at the central part of the detection area.
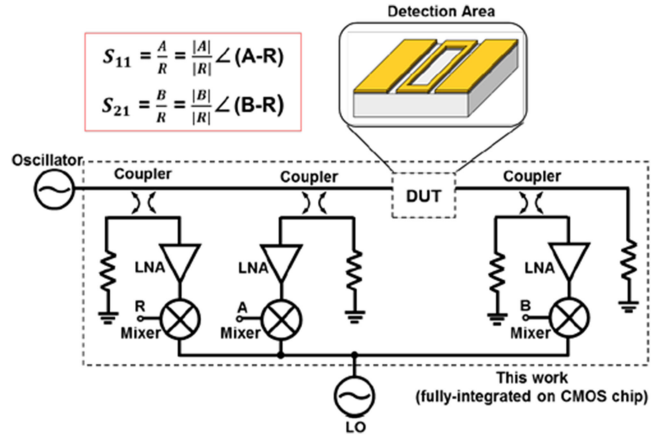


Fig. 4. Block diagram of a fully integrated VNA. The dashed line indicates the boundaries of the IC.

where $Y_2$ is the admittance of the detection window with CTCs/exosomes, surrounded by a red line in Fig. 2(c), and $\omega$ is an angular frequency of the input signal. From (2) and (3), it can be seen that $Y_2$, corresponding to types and the number of CTCs/exosomes, is related to the complex number of S-parameters such as $S_{11}$ and $S_{21}$, which means that the difference of CTCs/exosomes' types and number on the detection area results in S-parameters change.

The detection area was designed in such a way that EM waves can be applied to the detection window, enabling the waves to penetrate CTCs/exosomes significantly. To confirm the effectiveness of EM waves, EM simulation was performed with CST MW Studio. For the EM simulation, the detection area was modeled considering the IMD materials, for instance their thickness and dielectric constant and then simulated. Fig. 3(a) shows the top-down view of electrical field distribution for the detection area while Fig. 3(b) is a cross section image at the central part. It is observed that the electrical field sufficiently concentrates on the detection area, approximately $10^5$ V/m.

### B. Fully-Integrated CMOS-Based VNA Architecture

Fig. 4 presents a block diagram of the proposed fully integrated CMOS–based VNA with the detection area. The VNA consists of signal-separation devices and receivers for down-converting and detecting the signals. In Fig. 4, when an incident wave is applied to the VNA chip at a certain frequency, the

first directional coupler of the signal-separation devices split the incident and reference waves. Therefore, ignoring various parasitic reflections, the incident signal on the reference path can be expressed as follows:

$$S_{refe} = \kappa_{cou} + \tau_{cou}\Gamma_{cou}I_{cou} + \tau_{cou}{}^3\Gamma_{cou}I_{cou}, \quad (4)$$

where $\tau_{cou}$, $\kappa_{cou}$, and $\Gamma_{cou}$ represent the transmission, coupling, and reflection coefficients, respectively, and $I_{cou}$ represents isolation of the directional coupler; these values are assumed the same for all the couplers. Then, the second coupler is used to distinguish the incident wave from the reflection waves from the device-under-test (DUT), corresponding to the detection area in Fig. 2(a). Thus, the signal on the reflection path can similarly be shown to be

$$S_{refl} = \tau_{cou}I_{cou} + \tau_{cou}{}^2 S_{11}\kappa_{cou}. \quad (5)$$

Finally, the third coupler separates the waves transmitted through the detection area from the incident waves. Hence, the signal on the transmission channel is

$$S_{tran} = \tau_{cou}{}^2 S_{21}\kappa_{cou}. \quad (6)$$

These equations from (4) to (6) are calculated by the Kirchhoff's rules.

These signals are conveyed to the receivers using low-noise amplifiers (LNA) and Gilbert mixers for down-converting to a lower frequency and evaluating the signals, which yields R, A, and B of the reference, reflection, and transmission signals, respectively, as shown in Fig. 4. In other words, $S_{refe}$, $S_{refl}$, and $S_{tran}$ can be ideally exploited as R, A, and B, respectively. From (4), (5) and (6), assuming the directional couplers have high isolation coefficients, the S-parameters can ideally be obtained as follows:

$$S_{11} = \frac{A}{R} = \frac{|A|}{|R|}\angle(A - R) \quad (7)$$

$$S_{21} = \frac{B}{R} = \frac{|B|}{|R|}\angle(B - R) \quad (8)$$

where |X| and $\angle$X represent the amplitude and phase of the phasor signal. Besides, note that R, A, and B are the reference, reflection and transmission signals, respectively. According to (7) and (8), the S-parameters can be calculated from the amplitude ratio and phase difference between the outputs of A and R and those of B and R.

In the measurement, the amplitudes and phases of A, B, and R can be obtained as the output from the mixer. Thus, we can obtain S-parameters for analyzing CTCs and exosomes.

Following sub sections introduces design and explanation of the building blocks.

*1) Directional Coupler:* The directional coupler shown in Fig. 5 is designed for signal-separation; the coupler consists of two inductors and capacitors [15]. To provide a low reflection coefficient and high isolation, the following equations should
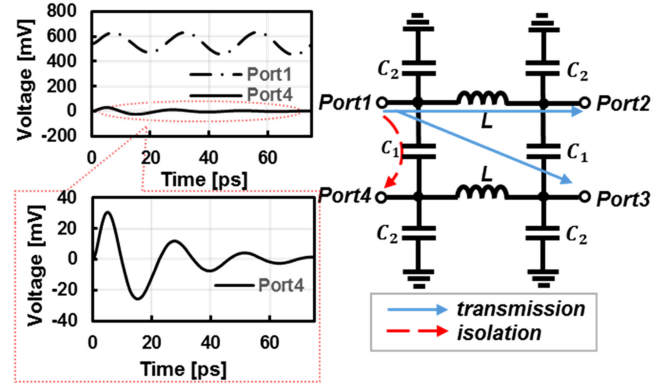


Fig. 5.   Schematic of the directional coupler and signal flow of input signal at port 1.
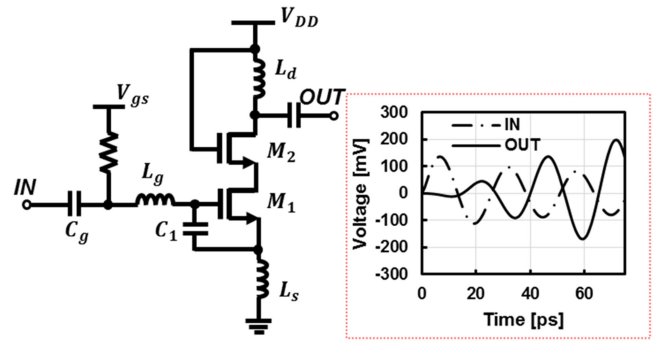


Fig. 6.   Schematic of the inductive source degeneration LNA.

be satisfied:

$$\omega_0{}^2 = \frac{1}{L(C_1 + C_2)} \quad (9)$$

$$2\omega_0{}^2 C_1 C_2 + \omega_0{}^2 C_2{}^2 = \frac{1}{Z_0{}^2} \quad (10)$$

where $\omega_0$ is the resonant frequency, and $Z_0$ represents the system impedance of 50 $\Omega$. The waveforms in Fig. 5 are from a simulation at 40 GHz, which illustrates that the signal at port 4 is isolated. Further information can be obtained from [15]. When a signal is input at port 1, the coupler isolates the signal at port 4 at a frequency determined by (9) while the other two ports receive transmitted waves. Owing to its reconfiguration, this property is true of input signals at other ports.

*2) LNA:* In order to achieve low noise and high gain, an inductive source degeneration LNA with a cascode transistor, as shown in Fig. 6, is applied. The transistor $M_1$ converts an input voltage into a current that stimulates an output voltage via $L_d$. In Fig. 6, $L_s$ is for input impedance matching whereas $L_g$ and $C_1$ are used to improve the noise performance [16].

*3) Gilbert Mixer:* Fig. 7 shows a schematic of a common single-ended Gilbert mixer for down-conversion and a spectrum waveform in simulation of input (IN) and local oscillator (LO) signals with frequencies of 40 GHz and 33 GHz, respectively. In Fig. 7, the frequencies $f_{IN}$ and $f_{LO}$ represent the frequencies of the IN and LO signals, respectively. The mixer can down-convert by switching the current caused by the IN voltage at the LO frequency, which generates signals multiplied with IN and

Fig. 7. Schematic of the single-ended Gilbert mixer and a spectrum waveform at simulation of a 40 GHz input.



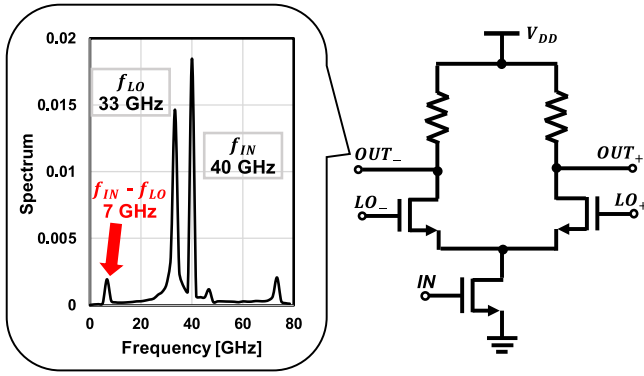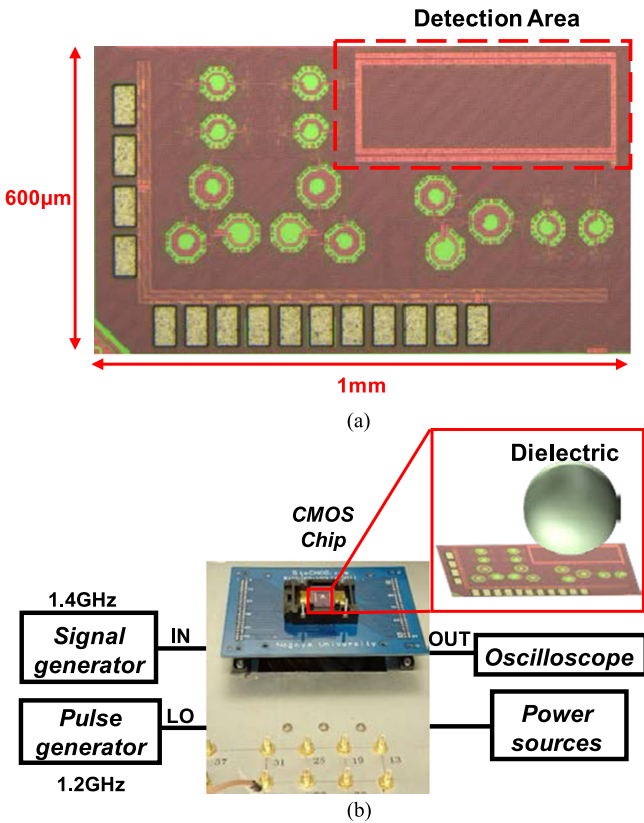Fig. 8. (a) Microphotograph of the test chip, (b) S-parameter measurement setup.

LO, producing outputs with the differential frequency between the IN and LO signals, $f_{IN} - f_{LO}$. As in the simulated spectrum waveform, the Gilbert mixer successfully outputs 7 GHz, which is equal to the frequency $f_{LO} = 33$ GHz subtracted from $f_{IN} = 40$ GHz. As mentioned in the latter measurement setup section, due to the limitation of I/O design and measurement setup, we have tested with 1.4 GHz input signal.

## III. TEST CHIP DESIGN AND MEASUREMENT SETUP

In order to validate the operation of the proposed system, a test chip was fabricated in 65-nm CMOS technology. Fig. 8(a) illustrates a microphotograph of the test chip. It occupies 600 $\mu$m

$\times$ 1 mm and contains the detection area surrounded by a red line, the on-chip VNA, and I/O pads. Fig. 8(b) represents the measurement setup for CTCs/exosomes dielectric characterization analysis. In this paper, owing to the limitation on I/O and measurement devices, a 1.4 GHz input signal and a 1.2 GHz signal are applied to the test chip, which is supposed to generate mixed output signals of 200 MHz. S-parameters were calculated based on (8) and (9) from the outputs R, A, and B. For measurements to validate the system's effectiveness, various dielectrics, for example water and magnetic beads, were used in the first step and then cells modeling CTCs were added in the next stage.

### A. Measurements Using Various Dielectrics

First of all, S-parameter measurements were conducted with the detection window on which a lump of silicone or a droplet of water (roughly 0.2 $\mu$L) were added. The silicone and water show 11.9 and 78 in the relative dielectric constant, respectively. Furthermore, to observe the S-parameter dependence on the concentrations, magnetic beads (Dynabeads M270) from 20 beads/$\mu$L to $2.2 \times 10^5$ beads/$\mu$L in concentration were used. In the measurements, the dropped volume including the magnetic beads was approximately 0.2 $\mu$L. The M270 consists of considerably cross-linked polystyrene and magnetic material, which have diameters of 2.8 $\mu$m. For the measurements, the procedure was conducted repeatedly three cycles for each dielectric to obtain the average value of the output signal amplitude. What is more, the two types of measurements were also performed using different test chips.

### B. Measurements Using CTCs Sample

In the next stage, samples modeling CTCs, lung cancer cells of H1975 and NCI-H82, were used in measurements. For the observation of the S-parameter dependence on the concentration, H1975 were set at concentrations from 50 cells/$\mu$L to $1.6 \times 10^4$ cells/$\mu$L, which are almost from 10 to $3.3 \times 10^3$ cells in the number of H1975.

In order to get the average statistic of the amplitude of the output signals, measurements for each type of cells were performed for five cycles. As with the measurement above, different chips were used in different measurements.

### C. Cells Growth

Fig. 9 shows the photograph of the cultured H1975 and NCI-H82 cells. The average diameters of the cultured H1975 and NCI-H82 cells are 11.7 $\mu$m and 12.5 $\mu$m, respectively. While, those of the dead H1975 and NCI-H82 cells are 9.9 $\mu$m and 6.3 $\mu$m, respectively. The survival rates of them are 62% and 98%, respectively.

## IV. RESULTS

### A. Measurements Results Using Various Dielectrics

Fig. 10 depicts the obtained waveforms of the reference voltage R and the reflection voltage A from the measurement, in which the waveforms of R and A are colored yellow and green,
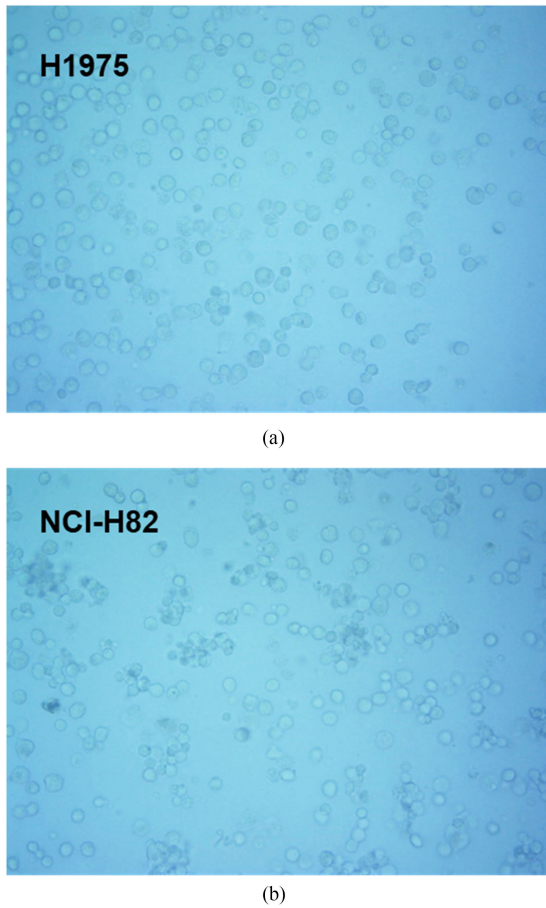
(a)



(b)

Fig. 9.    Photograph of the cultured cells (a) H1975 (b) NCI-H82.
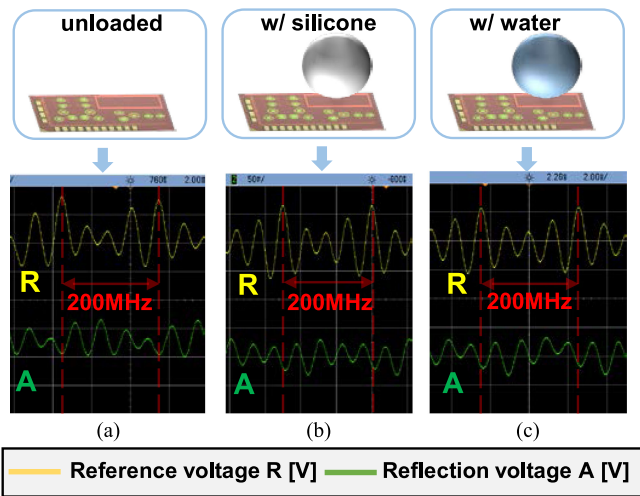


Fig. 10.    Measured waveforms of the reference voltage R and the reflection voltage A: (a) the unloaded detection area, (b) the detection area with a lump of silicone, and (c) the detection area with a water droplet.

respectively. In the measurement, there were three conditions of detection area: the unloaded detection area on which nothing was added, the detection area with the lump of silicone, and one with a droplet of water. From Fig. 10, it is clear that the output signals are successfully mixed to 200 MHz in frequency between the IN of 1.4 GHz and the LO of 1.2 GHz. Moreover,

TABLE II
MEASURED S-PARAMETERS FOR DIELECTRIC

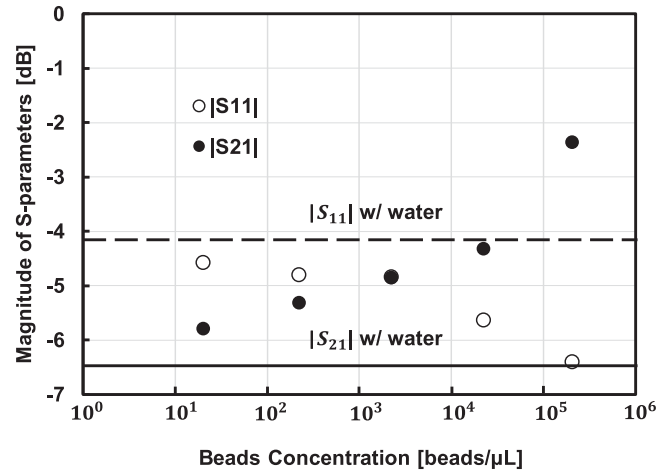| condition | $|S_{11}|$ [dB] | $|S_{21}|$ [dB] |
|---|---|---|
| unloaded | -5.31 | -3.10 |
| w/ silicone | -7.30 | -5.06 |
| w/ water | -6.09 | -9.14 |



Fig. 11.    S-parameters dependence on the concentration of the magnetic beads.

Fig. 10 also shows the change in amplitude of the reference and reflection waves. The measured and calculated S-parameters are summarized on Table II from the average values of the three runs of the measurements for each sample. In Table II, the change in $|S_{21}|$ becomes greater than $|S_{11}|$. The unloaded detection area shows rationally the smallest transmission coefficient $|S_{21}|$ of $-3.10$ dB. This is because microwave penetrates and is absorbed by dielectric on the detection window, resulting in the reduction of $|S_{21}|$ from the dielectric loss. Hence, water describes higher transmission loss of $-9.14$ dB than the attenuation of $-5.06$ dB for the silicone since the loss tangent, $\tan\delta$, of water is higher than silicone. Additionally, variations of around 20% and 50% in $|S_{21}|$ for the detection area with the silicone and the water are observed in Table II while there are changes of approximately 20% and 8.5% in $|S_{11}|$, respectively. To confirm the correct tendency for the dielectrics, the MWS simulation was performed, which offering the same relationship of the changes by both dielectrics as the measurements.

Fig. 11 represents the S-parameters dependence on the concentrations of the magnetic beads. The concentrations varied at 20, $2.2 \times 10^2$, $2.2 \times 10^3$, $2.2 \times 10^4$, and $2.2 \times 10^5$ beads/$\mu$L, corresponding to the estimation in the number of 4, $4.4 \times 10^1$, $4.4 \times 10^2$, $4.4 \times 10^3$, and $4.4 \times 10^4$ beads.

In Fig. 11, it is observed that there is the reduction in $|S_{11}|$ while there is the rise in $|S_{21}|$ along with the increase of the concentrations. The reason showing the relationship is the magnetic beads set on the detection window is inferior in dielectric
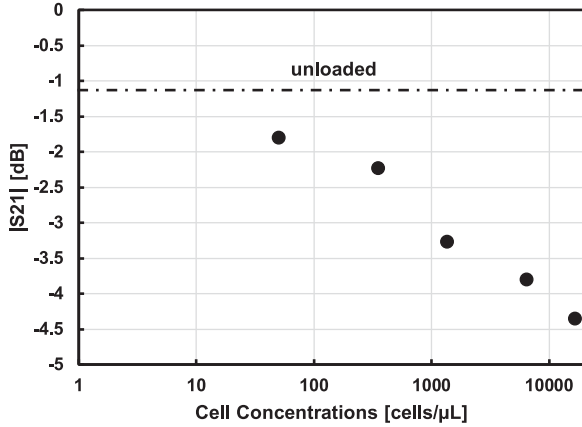
Fig. 12.    S-parameters dependence on the concentration of H1975.

characterization to water, which means that a small number of magnetic beads do not interfere with the dielectric property of water, getting closer to the value for water, $|S_{11}|$ of $-4.19$ dB and $|S_{21}|$ of $-6.55$ dB. The proposed system has the potential to analyze the magnetic beads even at low concentrations of 20 beads/$\mu$L compared to the S-parameters for water. Considering the measurement results above, the proposed fully-integrated system can analyze the dielectric characterization of dielectrics.

### B. Measurements Results Using CTCs Samples

As with the measurement using the magnetic beads mentioned above, the measurement using lung cancer cells named H1975 cells was performed, offering the result of the S-parameter dependence on the concentrations as shown in Fig. 12. The concentrations of H1975 set on the detection window were approximately 50, $3.5 \times 10^2$, $1.4 \times 10^3$, $6.4 \times 10^3$, and $1.6 \times 10^4$ cells/$\mu$L, which is almost estimated 10, 70, $2.7 \times 10^2$, $1.3 \times 10^3$, and $3.3 \times 10^3$ cells. According to Fig. 12, the S-parameter $|S_{21}|$ decreases as there is the increase in the concentrations of H1975 cells dropped on the detection area, which is the opposite tendency compared to the S-parameter dependence of the magnetic beads. This seems because the dielectric characterization of the cells is greater than the magnetic beads, meaning that the larger number of the cells show the greater transmission loss $|S_{21}|$. Fig. 12 depicts the proposed system is able to analyze the S-parameter dependence on concentration of the cells modeling CTCs, even at low concentrations of 50 cells/$\mu$L. From Fig. 12, the limitation on the H1975 detection of the proposed system can be assumed over 50 cells/$\mu$L, that is almost over 10 cells/$\mu$L.

Fig. 13 shows the waveforms of the reference voltage R and transmission voltage B, which are shown by the yellow and green line, respectively, when nothing and two CTCs-model cells of NCI-H82 and H1975 at 300 cells/$\mu$L were set on the detection window in order. As seen in the measurement for different dielectrics, it can be confirmed that the output signals of the reference voltage and transmission voltage have 200 MHz in frequency, generated from the 1.4 GHz input and 1.2 GHz LO with the mixer, from Fig. 13. The S-parameter were measured and calculated from the mixed output signals shown on Table III. In Table III, when setting NCI-H82 on the detection window,
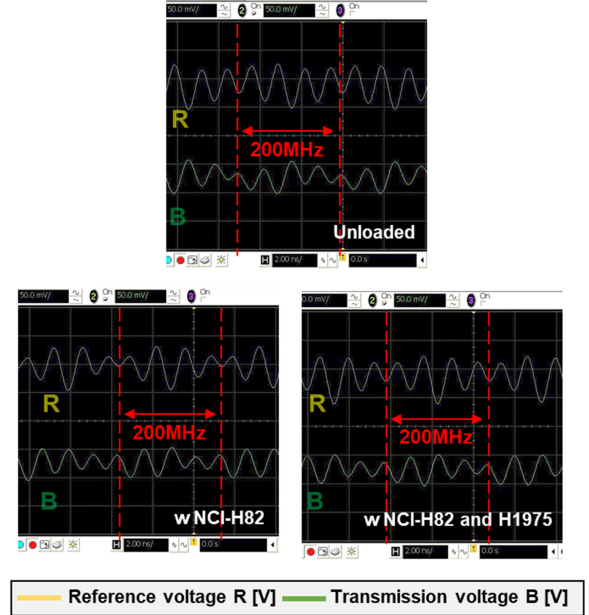


Fig. 13.    Output waveforms of the reference voltage R and the transmission voltage B for the unloaded, the detection area with the NCI-H82, and the detection area with the NCI-H82 and H1975 at 300 cells/$\mu$L.

TABLE III
MEASURED S-PARAMETERS FOR CANCER CELLS

| condition | $|S_{21}|$ [dB] |
|---|---|
| unloaded | -3.20 |
| w/ NCI-H82 | -4.50 |
| w/ NCI-H82 and H1975 | -5.50 |

there is the drop to $-4.50$ dB in the S-parameter compared to the unloaded, which has the lowest transmission loss of $-3.20$ dB. In addition, the drop of H1975 results in the $|S_{21}|$ degradation of $-5.50$ dB. The difference caused by the NCI-H82 cells is a little more significant than by the H1975 cells. The results of measurements using the real tumor cells modeling CTCs demonstrate that our proposed fully-integrated architecture can characterize the dielectric properties of cancer cells and has the potential in the application of the practical CTC and exosome analysis.

## V. DISCUSSION

This section discusses potential for analysis of exosome. Since exosomes are much smaller than cells, existing alternative CMOS-based methods such as DC current analysis with well structure [17], [18] cannot be applied. Thus, optical-based nanoparticle tracking analysis is widely used [19]. However, optical-based method requires large footprint and is not suitable for point-of-care testing applications.

TABLE IV
PERFORMANCE COMPARISON

|  | Previous work [13, IEEE TMTT 2016] | This work |
|---|---|---|
| Target | Circulating Tumor Cells (CTCs) | CTCs and exosomes |
| VNA Integration | Off-chip VNA | On-chip VNA |
| Frequency band | 40 GHz | 40 GHz |
| Feature | Flexibility | Low-noise, Small form factor |

In this study, due to the limitation of the sample preparation, only CTC measurements were performed. The diameters of exosomes are reported to be from 30 to 100 nm [20]. Thus, successful measurement of H1975 (11.7 $\mu$m diameter) with dynamic range of 320 (from 50 cells/$\mu$L to $1.6 \times 10^5$ cells/$\mu$L) imply the possibility of exosome analysis under high-concentration condition.

In order to realize exosome analysis under low-concentration condition, higher sensitivity and lower noise is desired. Due to the conservative design, we have not implemented any countermeasures such as the CDS. However, introduction of countermeasures will be helpful for exosome analysis.

Table IV summarizes the performance comparison. Our proposed work outperform the previous work from the viewpoint of noise performance and small form factor using on-chip VNA architecture.

Since the proposed architecture requires generating and handling millimeter wave signal, it also requires sophisticated instrumentations. However, signal generators, connectors, and cables are much cheaper than millimeter wave VNAs. Thus, the proposed work is more reasonable from the viewpoint of practical application. In addition, fortunately, recent progress on millimeter wave design for wireless communication will be helpful for addressing this matter.

## VI. CONCLUSION

Design and experimental demonstration of a fully-integrated CMOS circuit based on a vector network analyzer (VNA) and a transmission-line-based detection window for circulating tumor cell (CTC) and exosome analysis is presented. This is the first study in which an integrated VNA is designed with CMOS technology to process signals from CTC and achieve high integration between the VNA and the detection window. We confirmed that S-parameters depend on the type of dielectric and observed S-parameters measured with the proposed circuit for the change in dielectric constant; in particular, we observed $|S_{21}|$ degradations of $-1.96$ dB and $-6.04$ dB, which correspond to 20% and 50% reductions at 1.4 GHz, when a silicone resin lump and

a water droplet, respectively, were individually added on the detection window. Moreover, from another measurement using magnetic beads ranging in concentration from 20 beads/$\mu$L to $2.2 \times 10^5$ beads/$\mu$L, the measured S-parameters vary depending on the concentration of the magnetic beads, and even a low concentration of the beads can be detected with the detection window. In addition, the measurement results with CTC samples in concentration from 50 cells/$\mu$L to $1.6 \times 10^4$ cells/$\mu$L are demonstrated. These results demonstrated that our proposed system allows for dielectric characterization and presents the possibility of use in practical CTC and exosome analysis.

## REFERENCES

[1] M. R. Stratton, "Exploring the genomes of cancer cells: Progress and promise," *Science*, vol. 331, no. 6024, pp. 1553–155, Mar. 2011.
[2] R. F. Swaby and M. Cristofanilli, "Circulating tumor cells in breast cancer: A tool whose time has come of age," *BMC Med.*, vol. 9, no. 43, pp. 1–7, Apr. 2011.
[3] D. Marrinucci, "Fluid biopsy in patients with metastatic prostate pancreatic and breast cancers," *Phys. Biol.*, vol. 9, no. 1, pp. 1–9, Feb. 2012.
[4] M. C. Miller, G. V. Doyle, and L. W. Terstappen, "Significance of circulating tumor cells detected by the cellsearch system in patients with metastatic breast colorectal and prostate cancer," *J. Oncol.*, pp. 1–8, Jan. 2010, Art. no. 617421.
[5] A. M. Sieuwerts, "mRNA and microRNA expression profiles in circulating tumor cells and primary tumors of metastatic breast cancer patients," *Clin. Cancer Res.*, vol. 17, no. 11, pp. 3600–3618, Jun. 2011.
[6] E. Heitzer, S. Perakis, J. B. Geigl, and M. R. Speicher, "The potential of liquid biopsies for the early detection of cancer," *NPJ Precis. Oncol.*, vol. 1, no. 36, pp. 1–9, 2017.
[7] T. Hase *et al.*, "Development of microfluidic devices for rapid, low-cost detection of EGFR mutations in cytological samples from patients with lung cancer," in *Proc. 16th IASLC World Conf. Lung Cancer*, Sep. 2015, Paper P2.04-022.
[8] L. Y. Zhang, A. Landoulsi, C. Bounaix, and M. du Punch, "Label-free colorectal cancer cell line bio-sensing using RF resonator," in *Proc. Int. Solid-State Sens., Actuators, Microsyst, Conf.*, Jun. 2013, pp. 1194–1197.
[9] M. Rezaei, E. Ebrahimi, S. Naseh, and M. Mohajerpour, "A new 1.4 GHz soil moisture sensor," *Measurement*, vol. 45, no. 7, pp. 1723–1728, Aug. 2012.
[10] H. Lee *et al.*, "A planar split-ring resonator-based microwave biosensor for label-free detection of biomolecules," *Sens. Actuators B, Chem.*, vol. 169, pp. 26–31, Jul. 2012.
[11] A. Ebrahimi, W. Withayachumnankul, S. F. Al-Sarawi, and D. Abbott, "Microwave microfluidic sensor for determination of glucose concentrtion in water," in *Proc. IEEE 15th Mediterranean Microw. Symp.*, Nov. 2015, pp. 1–3.
[12] H. W. Wu, "Label-Free and antibody-free wideband microwave biosensor for identifying the cancer cells," *IEEE Trans. Microw. Theory Tech.*, vol. 64, no. 3, pp. 982–990, Mar. 2016.
[13] T. Nakanishi, M. Matsunaga, A. Kobayashi, K. Nakazato, and K. Niitsu, "A fully-integrated circulating tumor cell analyzer using an on-chip vector network analyzer and a transmission-line-based detection window in 65-nm CMOS," in *Proc. IEEE Biomed. Circuits Syst. Conf.*, Oct. 2017, pp. 1–4.
[14] T. Nakanishi, M. Matsunaga, A. Kobayashi, K. Nakazato, and K. Niitsu, "A 40-GHz fully integrated circulating tumor cell analysis vector network analyzer in 65-nm CMOS technology with coplanar-line-based detection area," *Jpn. J. Appl. Phys.*, vol. 57, no. 3S2, Jan. 2018, Art. no. 03EC01.
[15] J. Sun and C. Li, "A highly reconfigurable low-power CMOS directional coupler," *IEEE Trans. Microw. Theory Techni.*, vol. 60, no. 9, pp. 2815–2822, Sep. 2012.

[16] X. Fan, H. Zhang, and E. Sánchez-Sinencio, "A noise reduction and linearity improvement technique for a differential Cascode LNA," *IEEE J. Solid-State Circuits*, vol. 43, no. 3, pp. 588–599, Mar. 2008.

[17] K. Niitsu, S. Ota, K. Gamo, H. Kondo, M. Hori, and K. Nakazato, "Development of microelectrode arrays using electroless plating for CMOS-Based direct counting of bacterial and HeLa cells," *IEEE Trans. Biomed. Circuits Syst.*, vol. 9, no. 5, pp. 607–619, Nov. 2015.

[18] T. Kuno, K. Niitsu, and K. Nakazato, "Amperometric electrochemical sensor array for on-chip simultaneous imaging," *Jpn. J. Appl. Phys.*, vol. 53, Feb. 2014, Art. no. 04EL01.

[19] V. Filipe, A. Hawe, and W. Jiskoot, "Critical evaluation of nanoparticle tracking analysis (NTA) by NanoSight for the measurement of nanoparticles and protein aggregates," *Pharmaceutical Res.*, vol. 27, no. 5, pp. 796–810, May 2010.

[20] V. R. Minciacchi, M. R. Freeman, and D. D. Vizio, "Extracellular vesicles in cancer: Exosomes, microvesicles and the emerging role of large oncosomes," *Seminars Cell Dev. Biol.*, vol. 40, pp. 41–51, Feb. 2015.

**Kiichi Niitsu** (S'05–M'10) was born in Japan, in 1983. He received the B.S. (*summa cum laude*), M.S., and Ph.D. degrees in electrical engineering from Keio University, Yokohama, Japan, in 2006, 2008, and 2010, respectively.

From 2010, he was an Assistant Professor with Gunma University, Kiryu, Japan. Since 2012, he has been a Lecturer with Nagoya University, Nagoya, Japan. Since 2018, he has been an Associate Professor with Nagoya University. From 2015 to 2019, he serves concurrently as a Precursory Research for Embryonic Science and Technology Researcher, Japan Science and Technology Agency. From 2008 to 2010, He was a Research Fellow (DC1) of the Japan Society for the Promotion of Science, a Research Assistant of the Global Center of Excellence Program at Keio University and a Collaboration Researcher of the Keio Advanced Research Center. He has authored or coauthored 54 referred original journal papers, 112 international conference papers, 6 patents, and 4 book chapters including 3 TBioCAS, 1 TCAS-I, 5 JSSC, 5 TVLSI, 2 ISSCC, 4 Symp. on VLSI Circuits, 13 BioCAS, 1 ISCAS, 1 CICC, 1 MEMS, 4 A-SSCC, 9 APCCAS, 2 ICECS. His current research interests include the low-power and high-speed technologies of analog and digital VLSI circuits for biomedical application.

Dr. Niitsu was the recipient of the 2006 KEIO KOUGAKUKAI Award, the 2007 INOSE Science Promotion Award, the 2008 IEEE SSCS Japan Chapter Young Researcher Award and the 2009 IEEE SSCS Japan Chapter Academic Research Award both from IEEE Solid-State Circuits Society Japan Chapter, the 2008 FUJIWARA Award from the FUJIWARA foundation, 2011 YASUJIRO NIWA Outstanding Paper Award, 2011 FUNAI Research Promotion Award, 2011 Ando Incentive Prize for the Study of Electronics, 2011 Ericsson Young Scientist Award, 2012 ASP-DAC University LSI Design Contest Design Award, NF Foundation R&D Encouragement Award, AKASAKI Award from Nagoya University, IEEE Nagoya Section Young Researcher Award, IEEE Biomedical Circuits and Systems Conference 2016 (BioCAS 2016) Best Paper Award, the 2017 Commendation for Science and Technology by the Minister of Education, Culture, Sports, Science and Technology, the Young Scientists' Prize, the IEICE SUEMATSU YASUHARU Award, and the IEEE Biomedical Circuits and Systems Conference 2018 (BioCAS 2018) Best Live Demonstration Award. He served as a technical committee of IEEE biomedical circuits and systems (BioCAS TC), a Review Committee Member of ISCAS 2017/2018/2019, a Technical Program Committee of ICECS 2018, a Review Committee Member of APCCAS 2014, an editorial committee of IEICE Transactions on Electronics, Special Section on Analog Circuits and Related SoC Integration Technologies, and an editorial committee of IEICE ESS Fundamental Review. He is a member of IEEE, IEICE (the Institute of Electronics, Information and Communication Engineers of Japan), and JSAP (the Japan Society of Applied Physics).

**Taiki Nakanishi** was born in Japan. He received the B.S. degree in electrical engineering and computer science, in 2017, from Nagoya University, Nagoya, Japan, where he is currently working toward the M.S. degree in CMOS biosensor design.

His research interest is focused on mixed-signal CMOS integrated circuits for biomedical applications.

**Shunya Murakami** was born in Japan in 1996. He is currently working toward the M.S. degree in electrical engineering and computer science with Nagoya University, Nagoya, Japan. His research interest is focused on mixed-signal CMOS integrated circuits for biomedical applications.

**Maya Matsunaga** was born in Japan. She received the B.S. degree in electrical engineering and computer science, in 2017, from Nagoya University, Nagoya, Japan, where she is currently working toward the M.S. degree. Her research interest is focused on mixed-signal CMOS integrated circuits for biomedical applications.

**Atsuki Kobayashi** (S'16) was born in Yamanashi, Japan in 1993. He received the B.S. degree, in 2016, in electrical engineering and computer science from Nagoya University, Nagoya, Japan, where he is currently working toward the M.S. degree in CMOS biosensor design.

His research interest is focused on mixed-signal CMOS integrated circuits for biomedical applications. Mr. Kobayashi was the recipient of the IEEE BioCAS 2016 Best Paper Award.

**Nissar Mohammad Karim** was born in Bangladeshi in 1985. He received the B.E. degree in electrical and electronic engineering from American International University-Bangladesh, Dhaka, Bangladesh, the M.S. degree in microengineering and nanoelectronics from National University of Malaysia, Bangi, Malaysia, and the Ph.D. degree in material science and microelectronics from University of Malaya, Kuala Lumpur, Malaysia.

From 2015, he has been in Venture Business Laboratory, Nagoya University, Japan as a Post-Doctor Researcher. He is currently the Researcher with CREST, JST. His research interest is microelectronics including CMOS circuit design for biomedical applications.
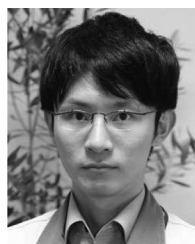
**Jun Ito** was born in Japan in 1987. He received B.E. and M.S. degrees in mechanical engineering from Nagoya University, Nagoya, Japan, in 2010 and 2012, respectively. He was with AGC, Inc., Tokyo, working on research and development of glass production technology, especially in glass processing, tempering, and printing. His main concerns are glass micro fabrication using ultra short pulse laser for biomedical applications.

**Naoya Ozawa** was born in Nagoya, Japan, in 1983. He received the MBBS degree from Nagoya University, Nagoya, Japan, in 2008. He was with Nagoya Ekisaikai Hospital, Aichi, Japan, as a Medical Doctor. In 2014, he moved to Chutoen General Hospital, Shizuoka, Japan. Since 2016, he has been a student of the Graduate School of Medicine, Nagoya University. His research activity is mainly focused on liquid biopsy in lung cancer.
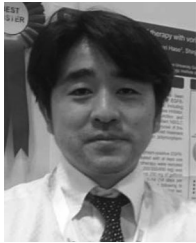
**Tetsunari Hase** was born in Japan in 1976. He received the Ph.D. degree from Nagoya University, Nagoya, Japan, in 2011. He is currently an Assistant Professor with the Department of Respiratory Medicine, Nagoya University. He received a medical license in 2001. His main concern is development of new technologies and methods for detecting circulating tumor cell, cell-free DNA, and low-abundance proteins in blood collaborating with Nagoya University Engineering School and AGC, Inc.
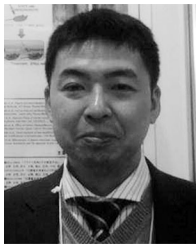
**Hiromasa Tanaka** was born in Japan in 1976. He received the B.S., M.S., and Ph.D. degrees in physics from the University of Tokyo, Tokyo, Japan, in 1999, 2001, and 2004, respectively. He was with the Yi Lab, University of California, Irvine, working on systems biology that focuses on complex interactions within biological systems, from 2004 to 2010. He studied the yeast mating signaling systems. To study functional genomics that is a field of systems biology that attempts to make use of the vast wealth of data produced by genomic projects, he moved to the Boone and Moffat Lab, University of Toronto, during 2010–2011. He was involved in a big project to identify cancer therapeutic targets by synthetic lethal screens using lentivirus-based shRNA knock-down library. Then, he came to the Hori Lab, Nagoya University, to study his current joint project, plasma medicine. He is working on cancer therapy using non-thermal atmospheric pressure plasma. He has found selective killing of glioblastoma brain tumor cells using plasma-activated medium and proposed the intracellular molecular mechanisms.

**Mitsuo Sato** was born in Japan. He received the Ph.D. degree from Nagoya University, Nagoya, Japan. He is currently a Professor with the Department of Pathophysiological Laboratory Sciences, Nagoya University Graduate School of Medicine. He has received a medical license. His main concern is clinical medicine of internal medical/respiratory medicine and oncology/tumor biology.

**Hiroki Kondo** was born in Okazaki, Japan, in 1971. He received the B.E., M.E., and Ph.D. degrees in the area of material science, from Nagoya University, Nagoya, Japan, in 1994, 1996, and 1999, respectively. He joined Fujitsu Corporation starting a research on reliability technology for multilayer interconnects in ULSI. He returned back to Nagoya University as an Assistant Professor and started a research on high-k/metal gate stack technologies. Especially, he focused on plasma nitridation processes. He have also studied formation processes of high-k gate stack structures using scanning tunneling microscopy, transmission electron microscopy, and synchrotron hard-X-ray photoelectron spectroscopy. He joined plasma nanotechnology research center, Nagoya University, in 2009, and started a research on high-density radical source and its application to nitride semiconductor growth. He also studies advanced plasma processes for nanomaterials and nanodevices, especially carbon nanomaterials and their applications. He had 37 invited talks in international conferences and authored or coauthored more than 110 of international academic journal papers.

**Kenji Ishikawa** is currently with the Plasma Medical Science Global Innovation Center and the Plasma Nanotechnology Research Center, Department of Engineering, Nagoya University, Nagoya, Japan. He is currently a Research Professor with Nagoya University. His main concerns are plasma biochemistry, biology, medicine, and agriculture, plasma etching and nanoscale processing technology, and nanographene synthesis.

**Hidefumi Odaka** was born in Japan in 1966. He received the Ph.D. degree from the Tokyo University, Tokyo, Japan, in 1997, studying a first-principle calculation method. He is currently a Senior Manager with AGC, Inc., working on the development of functional thin-film material and new plasma process for glass. He is currently with Nagoya University as a Specially Appointed Professor, studying a biochip.

**Yoshinori Hasegawa** received the Graduate degree from the University of Tokushima, Tokushima, Japan, in 1980, and the Ph.D. degree from the Nagoya University Graduate School of Medicine, Nagoya, Japan, in 1987. He is currently a Professor and the Chairman of Department of Respiratory Medicine, Nagoya University Graduate School of Medicine, Nagoya, Japan. He was with the Department of Microbiology and Immunology, UCLA, as a Research Fellow, from 1987 to 1989. He was appointed to the present position in 2007. His specialties and research fields of interest are molecular mechanisms of respiratory diseases, treatment of lung cancer, tumor immunology, and pharmacogenomics. He is the Chairman of the Board of Directors of the Japanese Respiratory Society and the Vice-Chairman of the Board of Directors of the Japanese Society of Internal Medicine.

**Masaru Hori** was born in Gifu, Japan, in 1958. He received the B.E. and the M. Tech. degrees from the Department of Electric Engineering from Waseda University, Tokyo, Japan, in 1981 and 1983, respectively, and the Ph.D. degree from the Department of Electric Engineering from Nagoya University, Nagoya, Japan, in 1986. In 1986, he joined Toshiba Corporation, Kawasaki, Japan. Since 1992, he has been with the Graduate School of Engineering, Nagoya University. He became a Research Associate in 1992, an Assistant Professor in 1994, an Associate Professor in 1996, a Researcher, Cavendish Laboratory, University of Cambridge, U.K., in 1997, and a Professor in 2004. He was a Vice Director, Plasma Nanotechnology Research Centre, Nagoya University, in 2007, a Director, Plasma Nanotechnology Research Centre, Nagoya University, in 2009, and a Director with Plasma Medical Science Global Innovation Centre, Nagoya University, in 2013. His current research interests include plasma electronics, plasma processing science in materials and devices, and plasma life sciences to medicine and agriculture. Dr. Hori is a Fellow of The Japan Society of Applied Physics. He was the recipient of Prize for Science and Technology, by the Minister of Education, Culture, Sports, Science and Technology, Japan in 2011, Prize for Industry-Government-Academia cooperation person of merit, Science and Technology Minister Policy Award, Japan, in 2011, and the 14th Plasma Material Science Award, Division of 153 Committee, Japan Society for the Promotion of Science, Japan, in 2012.

**Kazuo Nakazato** was born in Japan on 18 October, 1952. He received the B.S., M.S. and Ph.D. degrees in physics from the University of Tokyo, Tokyo, Japan, in 1975, 1977, and 1980, respectively. In 1981, he joined the Central Research Laboratory, Hitachi Ltd., Tokyo, Japan, working on high-speed silicon self-aligned bipolar devices SICOS (sidewall base contact structure), which were adopted in main frame computer Hitachi M-880/420. In 1989, he moved to Hitachi Cambridge Laboratory, Hitachi Europe Ltd., Cambridge, U.K., as a Senior Researcher and a Laboratory Manager, working on experimental and theoretical study of quantum electron transport in semiconductor nano structures, including single-electron memory. Since 2004, he has been a Professor of intelligent device with the Department of Electrical Engineering and Computer Science, Graduate School of Engineering, Nagoya University, Nagoya, Japan. His main concerns are BioCMOS technology, single molecule-CMOS hybrid devices, and CMOS analog circuits for integrated sensors.